Abdel-Malek, K., (1996), "Criteria for the Locality of a Manipulator Arm with Respect to an Operating Point," *IMEChE Journal of Engineering Manufacture*, Vol. 210 (1), pp. 385-394.

Criteria for the locality of a manipulator arm with respect to an operating point

K Abdelmalek, BSc, MSc, PhD
Department of Mechanical Engineering and Center for Computer Aided Design
The University of Iowa, Iowa City, IA 52242, USA.

ABSTRACT

Criteria for determining an optimum locality of a manipulator arm is developed. Often times in a manufacturing environment, the tools, fixtures, and targets that a manipulator has to deal with cannot be relocated. Thus, the choice of the manipulator locality is important. The method presented in this paper uses the notion of a service sphere to determine required orientability at an operating point. The boundary surfaces to the wrist-accessible output set is determined and positioned such that the service sphere is inside the wrist-accessible output set.

To determine boundary surfaces of the wrist-accessible output set, manipulator singularities (internal, boundary, and higher order) are computed and substituted into the constraint equation to parametrize singular surfaces. Part of these surfaces may lie internal to the boundary while other parts are a subset of the boundary. Singular surfaces are then intersected to determine second-order singularities. Second-order singularities partition surfaces into subsurfaces. Those subsurfaces on the boundary are determined by perturbing a point on the surface and concluding whether the perturbed point satisfies the constraint equations. The boundary to the wrist-accessible output set is then located with respect to the service sphere. The locality of the manipulator is determined for maximum orientability.

1 PROBLEM STATEMENT

Given an operating point at which a manipulator is required to have most orientability, it is necessary to locate (place) the manipulator such that maximum orientability is achieved. Optimized locality in this paper is defined as a subset of the position and orientation of a manipulator that provides maximum orientability with respect to an operating point. This is achieved by developing criteria for the location of the manipulator base.

A general method used to automatically determine the placement of manipulators to optimize multiple "kinematic performance" was presented by Zeghloul and Pamanes-Garcia **(1)**. In this method, the task to be accomplished by the manipulator is specified by defining the Cartesian position of the end-effector for a certain number of path points. An optimization criteria is assigned to each point. A search for the placement optimizing all criteria is carried out. Another method is to locate assembly tasks in the manipulator workspace in order to optimize the maniputability index **(2)**.

In manufacturing environments, the problem can be addressed by using rules of thumb, trial and error, or by locating the target "deep" inside the workspace. Determination of manipulator workspace has been addressed by many investigators in recent years. The term service sphere **(3)**

provides an indication of manipulator performance. A study on the relationship between the kinematic geometry and manipulator performance including workspace was presented by Roth **(4)**. A numerical approach to this problem was formulated and solved via tracing boundary surfaces of a workspace **(5)**. The accessible regions of planar manipulator **(6)** and the effect of hand size on workspace were also analytically studied **(7)**.

Recently, numerical criteria to find the accessible output set **(8)** of a general multi-degree-of-freedom (DOF) system via analysis of its Jacobian were presented **(9)**. The algorithm computes tangent vectors at bifurcation points of continuation curves that define the boundary of manipulator workspaces. A cross-section of the workspace is performed and boundary continuation curves are traced. The method, demonstrated for closed-loop mechanisms, is problematic at higher-level bifurcation points such as wrist-singularities. The original computational method was presented by Wang and Wu **(10)**. This analysis using continuation curves at bifurcation points was used to study the workspace of the Stewart platform **(11)**.

The dexterous workspace of a manipulator as defined by Kumar and Waldron (1981) is a subspace of the accessible output set within which a vector on the end-effector may assume all orientations. The dexterous workspace was theoretically defined for a special case of manipulators with wrists having a full range of orientations **(12**, **13)**. Other methods of evaluating functionality of manipulators indicating a measure of dexterity at a target was presented **(14)**. Numerical criteria for mapping dexterous charts depicting all possible orientations at a target was addressed **(15)**. Other manipulator dexterity studies are presented by Qiu, Luh, and Haug **(11)**, Gosselin and Angeles **(17)**, and Emiris **(18)** . Studies of workspace and dexterity of parallel manipulators are reported by Agrawal **(20)** and Gosselin and Angeles **(17)**.

The method presented is demonstrated for a six DOF manipulator. Joints treated in this paper are either prismatic or revolute with generalized coordinates $\mathbf{q} = [q_1, q_2, q_3]^T \in R^3$, which are used to characterize the configuration (position and orientation) of each link in the manipulator.

It is noted that a solution to determining an optimized locality is not unique. To illustrate this, Fig. 1 depicts an operating point consisting of a dieset used for the manufacturing of miniature components. The dieset is constrained in terms of location since it has to be inside a press (not shown). The manipulator is required to pick-and-place a variety of components into the dieset with different configurations. Thus, orientability at the dieset is critical. Figures 1a and 1b show two of many valid solutions.

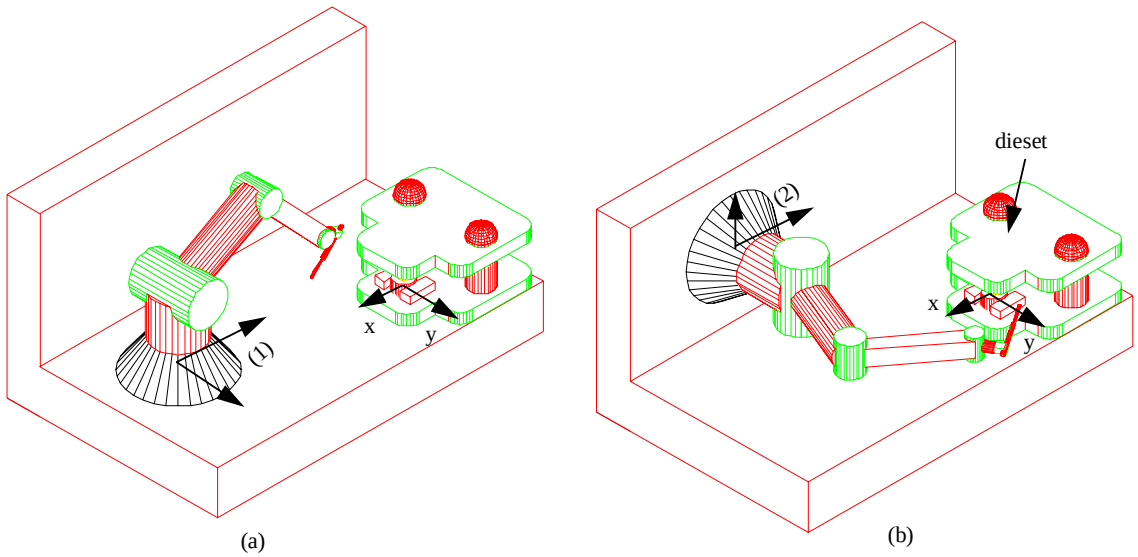

Fig. 1 (a) Manipulator base at locality 1 and
(b) manipulator base at locality 2

2 GENERAL PROCEDURE

The general procedure for determining an optimized locality consists of four steps.

(1) Locate a triad at the operating point **q** and establish a reference frame. Establish a service sphere with center at the operating point **q** such that service regions are defined on the surface of the sphere (Fig. 2). A service region is an area on the surface through which the end-effector may penetrate. The service sphere is used to indicate dexterity. The surface of the service sphere is parametrized as $\mathbf{x}_{ss}(u,v)$ centered at an operating point **q**. The service sphere can assume any radius less than the length of the last link of the manipulator. The terms "service sphere" and "service angle" were first introduced by Vinagradov **(3)**.

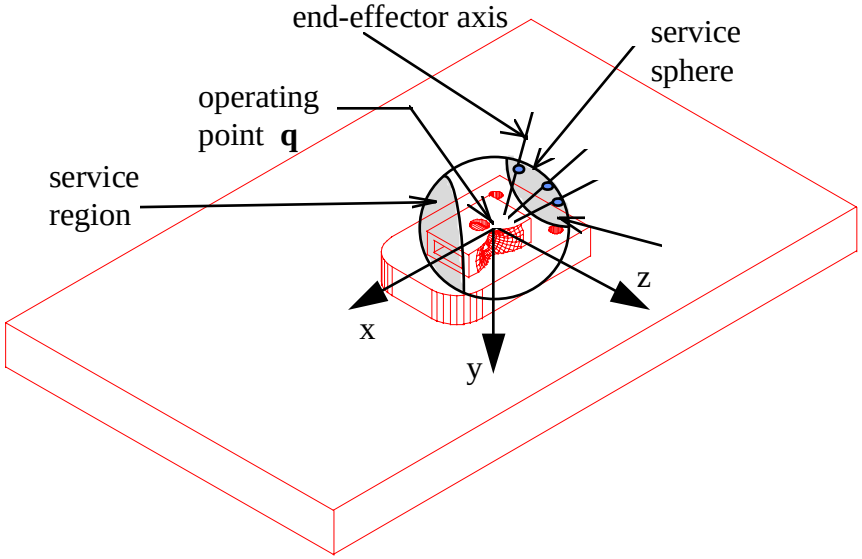

Fig. 2 A service sphere depicting a service region

(2) Partition the manipulator into two segments--one that locates the wrist point **w**, and another that controls the orientation of the wrist. The kinematics of positioning of the wrist point are readily available by use of the Denavit-Hartenberg representation (D-H) **(21)**. The D-H representation provides a systematic method for describing the relationship between adjacent links. The 4×4 transformation matrix describing a transformation from link (i-1) to link i for a revolute joint is

$$ {}^{i-1}\mathbf{T}_i = \begin{bmatrix} \cos\theta_i & -\cos\alpha_i \sin\theta_i & \sin\alpha_i \sin\theta_i & a_i \cos\theta_i \\ \sin\theta_i & \cos\alpha_i \cos\theta_i & -\sin\alpha_i \cos\theta_i & a_1 \sin\theta_i \\ 0 & \sin\alpha_i & \cos\alpha_i & d_i \\ 0 & 0 & 0 & 1 \end{bmatrix} \qquad (1) $$

where θ_i (depicted in Fig. 3a) is the joint angle from $\mathbf{x}_{i-1}$ to the $\mathbf{x}_i$ axis; d_i is the distance from the origin of the (i-1)th coordinate frame to the intersection of the $\mathbf{z}_{i-1}$ axis with the $\mathbf{x}_i$; a_i is the offset distance from the intersection of the $\mathbf{z}_{i-1}$ axis with the $\mathbf{x}_i$ axis; and α_i is the offset angle from the $\mathbf{z}_{i-1}$ axis to the $\mathbf{z}_i$ axis.

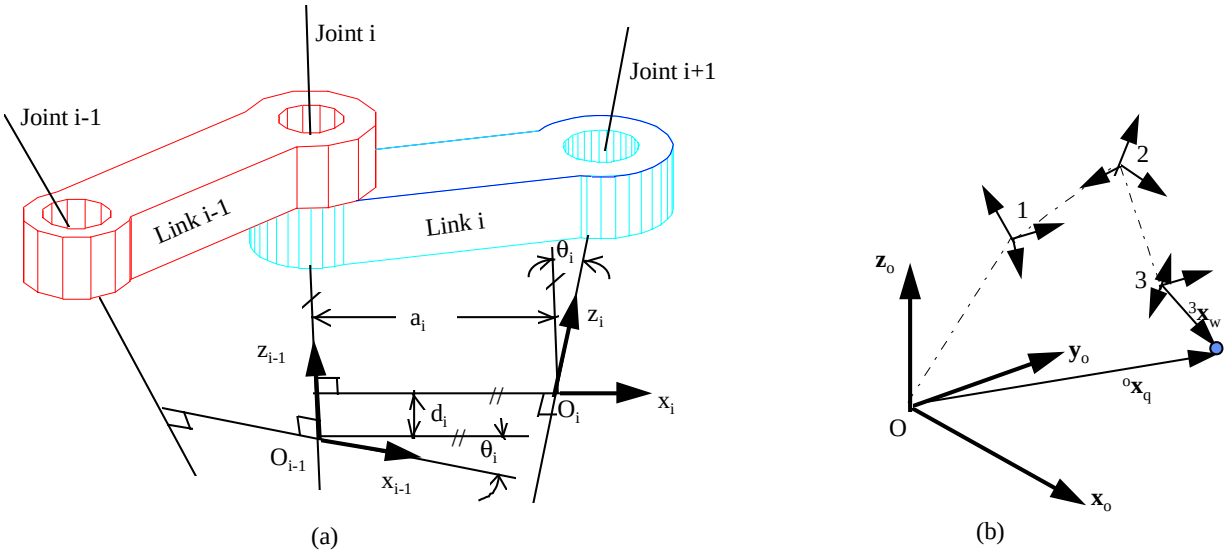

Fig. 3 (a) D-H representation, (b) Notation used in obtaining the wrist-accessible output set

The homogeneous transformation matrix ${}^0\mathbf{T}_i$ that specifies the configuration of the ith frame with respect to the base coordinate system is the product of successive transformation matrices of ${}^{i-1}\mathbf{T}_i$, such that

$$ {}^0\mathbf{T}_i = {}^0\mathbf{T}_1\,{}^1\mathbf{T}_2 \ldots {}^{i-1}\mathbf{T}_i = \prod_{j=1}^{i} {}^{j-1}\mathbf{T}_j \qquad (2) $$

where i is the number of degrees-of-freedom and ${}^{i-1}\mathbf{T}_i$ is of the form

$$ {}^{i-1}\mathbf{T}_i = \begin{bmatrix} {}^{i-1}\mathbf{R}_i & {}^{i-1}\mathbf{p}_i \\ 000 & 1 \end{bmatrix} \qquad (3) $$

where ${}^{i-1}\mathbf{R}_i$ is the rotation matrix between frame *i-1* and frame *i* and ${}^{i-1}\mathbf{p}_i$ is the position vector from the origin of the *i-1* frame to the *ith* frame. Thus, a six-axis manipulator with a

spherical wrist may be partitioned using the homogeneous transformation matrix relating the end-effector and the wrist to the reference frame such that

$$ {}^0\mathbf{T}_6 = {}^0\mathbf{T}_3\,{}^3\mathbf{T}_6 \tag{4} $$

The vector ${}^o\mathbf{x}_q$ describes the wrist-accessible output set of the wrist point such that

$$ {}^0\mathbf{x}_q = {}^0\mathbf{R}_3\,{}^3\mathbf{x}_w + {}^0\mathbf{p}_3 \tag{5} $$

where ${}^3\mathbf{x}_w$ is the vector describing the wrist point resolved in the reference frame of link 3 (Fig. 3b). In order to determine the boundary of the wrist-accessible output set for a mechanism, it has been shown that singularities (both internal and boundary) can be computed by proper manipulation of the Jacobian of the mechanism **(22)**. In this paper, first- and second-order singularities are computed. First-order singularities are substituted into the constraint equation to parametrize singular surfaces. Second-order singularities are subsequently computed and used to determine subsurfaces of the singular surfaces. Subsurfaces that are on the boundary of the wrist-accessible output set are identified. The set is then located with respect to the service sphere such that the sphere is totally inside the set. By doing so, it is evident that the manipulator will be able to have maximum orientability at the operating point.

For a given configuration of the manipulator, the generalized coordinates satisfy independent holonomic kinematic constraint equations of the form

$$ \Phi(\mathbf{q}) = {}^0\mathbf{x}_q - {}^0\mathbf{R}_3\,{}^3\mathbf{x}_w - {}^0\mathbf{p}_3 = 0 \tag{6} $$

where $\Phi: R^n \rightarrow R^l$ is a smooth function and l is the number of constraint equations. In addition, the generalized coordinates $\mathbf{q}$ are subject to inequality constraints representing joint limits.

$$ q_1^{\min} \le q_1 \le q_1^{\max} \tag{7a} $$

$$ q_2^{\min} \le q_2 \le q_2^{\max} \tag{7b} $$

$$ q_3^{\min} \le q_3 \le q_3^{\max} \tag{7c} $$

(3) Analytically determine a boundary to the wrist-accessible output set for the wrist point **w**. The constraint Jacobian of the constraint function $\Phi(\mathbf{q})$ of equation (6) for a certain configuration $\mathbf{q}^0$ is the 3×3 matrix

$$ \Phi_q(\mathbf{q}^0) = \left[\frac{\partial \Phi_i}{\partial q_j}\left(\mathbf{q}^0\right) \right] \tag{8} $$

The wrist-accessible output set is thus

$$ A = \left\{ {}^0\mathbf{x}_q \in R^n \colon \Phi(\mathbf{q}) = \mathbf{0}, \quad \text{for some } \mathbf{q} \right\} \tag{9} $$

The boundary of the wrist-accessible output set for a manipulator is a subset of the accessible output set at which the sub-Jacobian Φ_q of the kinematic constraint function of equation (6) is row-rank deficient **(23)**, i.e.,

$$ \partial A \subset \left\{ {}^o\mathbf{x}_q \in A \colon \operatorname{Rank}\Phi_q(\mathbf{q}) < l, \text{ for some } \mathbf{q} \right\} \tag{10} $$

For a three DOF mechanism (wrist-accessible output set), equating the determinant of the Jacobian to zero will result in the first-order singularities of the system. It is important to realize that some of these singularities will not satisfy the inequality constraints of the joint

variables **q**. To impose the inequality constraints, it is convenient to parametrize equation (7) by introducing new generalized coordinates λ_i such that an inequality constraint of the form

$$q_i^{\min} \le q_i \le q_i^{\max} \tag{11}$$

can be parametrized as

$$q_i = a_i + b_i \sin\lambda_i \tag{12}$$

where $a_i = \left(q_i^{\max} + q_i^{\min}\right)/2$ and $b_i = \left(q_i^{\max} - q_i^{\min}\right)/2$ are the mid point and half range of the inequality constraint. The Jacobian, with respect to the new coordinates, can be written as

$$\Phi_\lambda = \frac{\partial \Phi_i}{\partial q_j}\frac{\partial \mathbf{q}_j}{d\lambda_j} = \Phi_q \mathbf{q}_\lambda \tag{13}$$

First-order singularities are determined by equating the determinant of the Jacobian to zero such that

$$\mathbf{F}(\mathbf{x}) = \left|\Phi_q \mathbf{q}_\lambda\right| = 0 \tag{14}$$

Solving $\mathbf{F}(\mathbf{x})$ and substituting the results into equation (12), a set of first-order singularities μ_i *(i=1,...,m)* is generated, where *m* is the total number of singularities. First-order singularities generated by equation (14) are of two types: (1) i*nternal* singularities are those due to the assembly of the mechanism itself (2) *boundary* singularities are due to inequality constraints imposed on joints (e.g., space limitation, interference, and actuator capability).

Equation (14) is used to find the boundary of the wrist-accessible output set in closed form. Substituting each singularity into the wrist-accessible output set equation (5), a set of surfaces $\mathrm{X}^i(\mu_i)$ are parametrized such that

$$\mathrm{X}^i(\mu_i) = \left[\mathbf{x}^1(\mu_1), \mathbf{x}^2(\mu_2), \ldots, \mathbf{x}^m(\mu_m)\right] \tag{15}$$

where *i* = 1,...*m*. In determining accessible output sets, surfaces generated by singularities may intersect each other. Parts of a surface may be internal while other parts may be on the boundary of the wrist-accessible output set. Intersecting curves between surfaces determine a different type of singularity, which divide the surface into a number of subsurfaces. The set of generalized coordinates resulting from this intersection are called *second-order singularities* (the so-called bifurcation points on a cutting plane of the accessible output set). Pairs of surfaces are intersected such that

$$\mathbf{x}^i(\mu_i) - \mathbf{x}^j(\mu_j) = 0 \quad \text{for } i \ne j \tag{16}$$

Equation (16) may be carried out numerically. Continuation methods are used to compute the intersection curve **(24)**. Equation (16) will result in a number of second-order singularities. The number of singularities is augmented to μ_i, $i = 1,\ldots,m,m+1,\ldots,n$, where (*n*-*m*) is the number of surface intersections resulting in new singularities. The matrix of subsurfaces is augmented to

$$\Psi^i(\mu_i) = \left[\Psi^1(\mu_1), \Psi^2(\mu_2), \ldots, \Psi^m(\mu_m), \Psi^m(\mu_{m+1}), \ldots, \Psi^n(\mu_n)\right] \tag{17}$$

Equation (17) includes all subsurfaces due to internal, boundary, and second-order singularities. It remains to be determined whether these subsurfaces are internal or boundary surfaces. This can be performed by *perturbing* a known point on the subsurface and determining whether this point satisfies the equation of constraint (equation 6), subject to inequality constraints of equation (7). For a subsurface $\Psi^i(\mathbf{q})$, there are at least two

independent tangent vectors at the point $\mathbf{q}^o$ $\frac{\partial \Psi^i}{\partial q_1}$ and $\frac{\partial \Psi^i}{\partial q_2}$. The unit normal to the surface at a known point, where q_1 and q_2 are generalized coordinates **(25)**, is given as

$$\hat{\mathbf{n}}(\mathbf{q}^o) = \frac{\left(\frac{\partial \Psi^i}{\partial q_1} \times \frac{\partial \Psi^i}{\partial q_2}\right)}{\left\| \frac{\partial \Psi^i}{\partial q_1} \times \frac{\partial \Psi^i}{\partial q_2} \right\|} \tag{18}$$

For a small perturbation $\partial\varepsilon$ about the point $\mathbf{q}^o$ on the subsurface $\Psi^i(\mathbf{q})$ along the normal $\hat{\mathbf{n}}(\mathbf{q}^o)$, the coordinates of the perturbed point are

$$\mathbf{x} = \Psi^i(\mathbf{q}^o) \pm \partial\varepsilon\hat{\mathbf{n}}(\mathbf{q}^o) \tag{19}$$

For the perturbed point to exist inside the accessible output set, it has to satisfy equation (5), subject to inequality constraints of equation (7). Equating equation (5) to equation (19), a solution is sought to the following system of equations:

$$^0\mathbf{R}_3\,{}^3\mathbf{x}_w + {}^0\mathbf{p}_3 - \Psi^i(\mathbf{q}^o) \mp \partial\varepsilon\hat{\mathbf{n}}(\mathbf{q}^o) = \mathbf{0} \tag{20}$$

$$q_1^{\min} \le q_1 \le q_1^{\max} \tag{21a}$$

$$q_2^{\min} \le q_2 \le q_2^{\max} \tag{21b}$$

$$q_3^{\min} \le q_3 \le q_3^{\max} \tag{21c}$$

The subsurface $\Psi^i(\mathbf{q})$ is an internal surface if and only if there exists a solution for equation (20) for both perturbations $\pm\partial\varepsilon$, consistent with the inequalities of equation (21).

(4) Locate the wrist-accessible output set with respect to the service sphere such that the sphere is entirely inside the set. In step (4), the boundary of the wrist-accessible output set was generated (the boundary envelops the wrist workspace). This volume of space contains all accessible points by the wrist. On the other hand, the surface of a service sphere as defined by Vinagradov **(3)**, located at an operating point **q**, has all possible locations of the wrist points. That is, requiring the radius to equal that of the end-effector mandates that the service sphere must fall inside the wrist-accessible output set (i.e., the inside the boundary of the wrist-accessible output set).

3 EXAMPLE: A SIX-AXIS MANIPULATOR

Figure 4 depicts a six-DOF manipulator having three intersecting axes at **w** (called the wrist point). The wrist may be modeled as a spherical joint with center at **w (26)**.

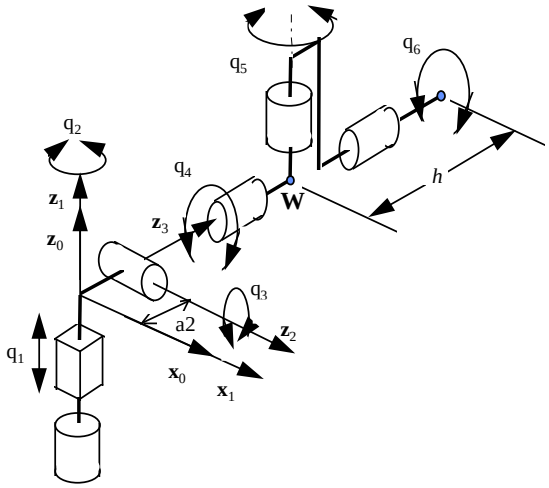

Fig. 4 A six-axis manipulator

To illustrate the foregoing analysis, partition the manipulator into two segments. The first segment of the manipulator comprises one prismatic and two revolute joints (Fig. 5a). The second segment is a spherical wrist (i.e., the end-effector may sweep a spherical surface centered at **w**)

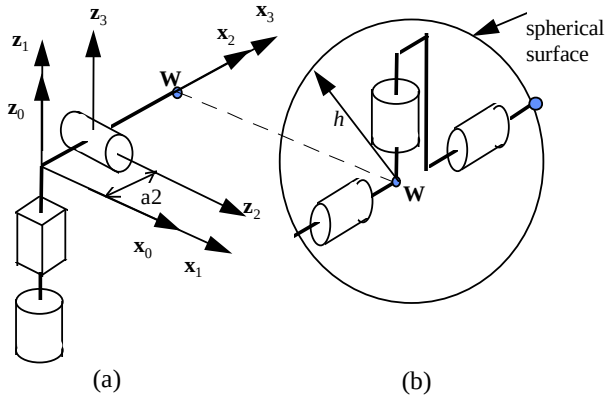

Fig. 5 (a) Three joints of a manipulator, (b) A spherical wrist (three intersecting axes)

It is required to determine an optimum locality for this manipulator with respect to an operating point **q** in its workspace. A sphere is set at **q** having radius *h*. For this manipulator, the three homogeneous transformation matrices (joints 1, 2, and 3) are

$$ {}^{0}\mathbf{T}_{1} = \begin{bmatrix} 1 & 0 & 0 & 0 \\ 0 & 1 & 0 & 0 \\ 0 & 0 & 1 & q_1 \\ 0 & 0 & 0 & 1 \end{bmatrix} \tag{22a} $$

$$ {}^{1}\mathbf{T}_{2} = \begin{bmatrix} \cos q_2 & 0 & \sin q_2 & 0 \\ \sin q_2 & 0 & -\cos q_2 & a_2 \sin q_2 \\ 0 & -1 & 0 & 0 \\ 0 & 0 & 0 & 1 \end{bmatrix} \tag{22b} $$

$$ {}^{2}\mathbf{T}_{3} = \begin{bmatrix} \cos q_3 & 0 & -\sin q_3 & 0 \\ \sin q_3 & 0 & \cos q_3 & 0 \\ 0 & -1 & 0 & 0 \\ 0 & 0 & 0 & 1 \end{bmatrix} \tag{22c} $$

where q_1, q_2, and q_3 are the generalized variables representing joint angles. Multiplying $\prod_{i=1}^{3} {}^{i}\mathbf{T}_{i-1}$, and extracting the rotation matrix (equation 3), we get

$$ {}^{0}\mathbf{R}_{3} = \begin{bmatrix} \cos q_2 \cos q_3 & -\sin q_2 & -\cos q_2 \sin q_3 \\ \sin q_2 \cos q_3 & \cos q_2 & -\sin q_2 \sin q_3 \\ \sin q_3 & 0 & \cos q_3 \end{bmatrix} \tag{23} $$

The position vector is

$$ {}^{0}\mathbf{p}_{3} = \begin{bmatrix} a_2 \cos q_2 & a_2 \sin q_2 & q_1 \end{bmatrix}^{T} \tag{24} $$

For a wrist point located at ${}^{3}\mathbf{x}_{w} = \begin{bmatrix} 0 & 0 & d_w \end{bmatrix}^{T}$, where d_w is the distance along the z-axis of the wrist point with respect to reference frame 3, the equation of constraint of the wrist point is

$$ \Phi(\mathbf{q}) = \begin{bmatrix} x - d_w \cos q_2 \cos q_3 - a_2 \cos q_2 \\ y - d_w \sin q_2 \cos q_3 - \sin q_2 a_2 \\ z - d_w \sin q_3 - q_1 \end{bmatrix} = \mathbf{0} \tag{25} $$

For the remainder of this discussion let $a_2 = 10$ and $d_w = 5$. This manipulator has joint constraints as follows

$$ 0 \le q_1 \le 20 \;\Rightarrow\; \mathrm{q}_1 = c_1 + c_2 \sin\lambda_1 = 10 + 10\sin\lambda_1 \tag{26} $$

$$ 0 \le q_2 \le 270^{o} \;\Rightarrow\; \mathrm{q}_2 = b_1 + b_2 \sin\lambda_2 = \frac{3\pi}{4} + \frac{3\pi}{4}\sin\lambda_2 \tag{27} $$

$$ -60^{o} \le q_3 \le 120^{o} \;\Rightarrow\; \mathrm{q}_3 = d_1 + d_2 \sin\lambda_3 = \frac{\pi}{6} + \frac{\pi}{2}\sin\lambda_3 \tag{28} $$

where the generalized coordinates λ_i were introduced according to equation (12). Evaluating the Jacobian of equation (14), we get

$$ \Phi_{\lambda} = \begin{bmatrix} 0 & -\sin(b_1 + b_2 \sin\lambda_2 b_2 \cos\lambda_2 \cos(d_1 + d_2 \sin\lambda_3) d_w - a_2 \sin(b_1 + b_2 \sin\lambda_2) b_2 \cos\lambda_2 \\ 0 & \cos(b_1 + b_2 \sin\lambda_2 b_2 \cos\lambda_2 \cos(d_1 + d_2 \sin\lambda_3) d_w - a_2 \cos(b_1 + b_2 \sin\lambda_2) b_2 \cos\lambda_2 \\ c_2 \cos\lambda_1 & 0 \end{bmatrix} $$

$$ \begin{matrix} -\cos(b_1 + b_2 \sin\lambda_2) \sin(d_1 + d_2 \sin\lambda_3) d_2 \cos\lambda_3 d_w \\ \sin(b_1 + b_2 \sin\lambda_2) \sin(d_1 + d_2 \sin\lambda_3) d_2 \cos\lambda_3 d_w \\ \cos(d_1 + d_2 \sin\lambda_3) d_2 \cos\lambda_3 d_w \end{matrix} \Bigg] \tag{29} $$

Internal and boundary singularities are computed by evaluating the determinant of the Jacobian and equating to zero

$$ \left|\Phi_{\lambda}\right| = c_2 \cos\lambda_1 \sin(d_1 + d_2 \sin\lambda_3) d_2 \cos\lambda_3 d_w b_2 \cos\lambda_2 \left(\cos(d_1 + d_2 \sin\lambda_3) d_w + a_2\right) = 0 \tag{30} $$

subject to constraint equations (26, 27, and 28). Singularities are determined by analyzing equation (30) as follows. The first term of equation (30), $\cos\lambda_1 = 0$, indicates that $\lambda_1 = \frac{\pi}{2}, -\frac{\pi}{2}$. Substituting λ_1 into equation (26) results in two singularities $q_1 = 0,\ 20$. For the term $\sin(d_1 + d_2 \sin\lambda_3) = 0$, indicates that $\sin(q_3) = 0$, i.e., two singularities $q_3 = 0,\ \pi$. For the term $\cos\lambda_3 = 0$, $\lambda_3 = \frac{\pi}{2}, -\frac{\pi}{2}$, i.e., two additional singularities $q_3 = -60^o,\ 120^o$. For the term $\cos\lambda_2 = 0\ \lambda_2 = \frac{\pi}{2}, -\frac{\pi}{2}$, i.e., two singularities $q_2 = 0,\ 270^o$. Finally, for the term $\cos(d_1 + d_2 \sin\lambda_3)d_w + a_2 = 0$, $\cos q_3 = -\frac{a_2}{d_w}$ will exist if and only if $a_2 < d_w$.

Note that only singularities that are consistent with the constraints are taken. The singularity ($q_3 = \pi$) is *not consistent with the constraints* (does not satisfy equation (28)) thus it is not considered. The total number of singularities is seven. Surfaces are parametrized by substituting each singularity into equation (25). For example, the torus $\mathbf{x}^2$ due to singularity $q_1 = 20$ is readily determined.

$$\mathbf{x}^2(q_1 = 20) = \begin{bmatrix} \cos q_2[d_w \cos q_3 + a_2] \\ \sin q_2[d_w \cos q_3 + a_2] \\ d_w \sin q_3 + 20 \end{bmatrix}, 0 \le q_2 \le 270^o \quad , \quad -60^o \le q_3 \le 120^o \qquad (31)$$

Similarly, a singular surface is parametrized for each first-order singularity such that

$$\mathbf{x}^1(q_3 = 120^o) = \begin{bmatrix} \cos q_2[-0.5d_w + a_2] \\ \cos q_2[-0.5d_w + a_2] \\ 0.866d_w + q_1 \end{bmatrix} 0 \le q_1 \le 20", \text{ and } 0 \le q_2 \le 270^o \qquad (32)$$

$$\mathbf{x}^3(q_3 = 0) = \begin{bmatrix} \cos q_2[d_w + a_2] \\ \cos q_2[d_w + a_2] \\ q_1 \end{bmatrix} 0 \le q_1 \le 20", \text{ and } 0 \le q_2 \le 270^o \qquad (33)$$

$$\mathbf{x}^4(q_3 = -60) = \begin{bmatrix} \cos q_2[0.5d_w + a_2] \\ \sin q_2[0.5d_w + a_2] \\ -0.866d_w + q_1 \end{bmatrix} \text{where, } 0 \le q_1 \le 20", \text{ and } 0 \le q_2 \le 270^o \qquad (34)$$

For surface $\mathbf{x}^5$, the parametrized surface is

$$\mathbf{x}^5(q_1 = 0) = \begin{bmatrix} \cos q_2[\cos q_3 d_w + a_2] \\ \sin q_2[\cos q_3 d_w + a_2] \\ \sin q_3 d_w \end{bmatrix} 0 \le q_2 \le 270^o \quad , -60^o \le q_3 \le 120^o \qquad (35)$$

$$\mathbf{x}^6(q_2 = 0) = \begin{bmatrix} d_w \cos q_3 + a_2 \\ 0 \\ d_w \sin q_3 + q_1 \end{bmatrix} 0 \le q_1 \le 20", \text{ and } -60^o \le q_3 \le 120^o \qquad (36)$$

$$\mathbf{x}^7(q_2 = 270^o) = \begin{bmatrix} 0 \\ -[d_w \cos q_3 + a_2] \\ d_w \sin q_3 + q_1 \end{bmatrix} 0 \le q_1 \le 20", \text{ and } -60^o \le q_3 \le 120^o \qquad (37)$$

Fig. 6a depicts each singular surface generated by the set of singularities. The union of these surfaces envelops the accessible set also shown in Fig 6a. Figure 6b is a cross section of the surfaces.

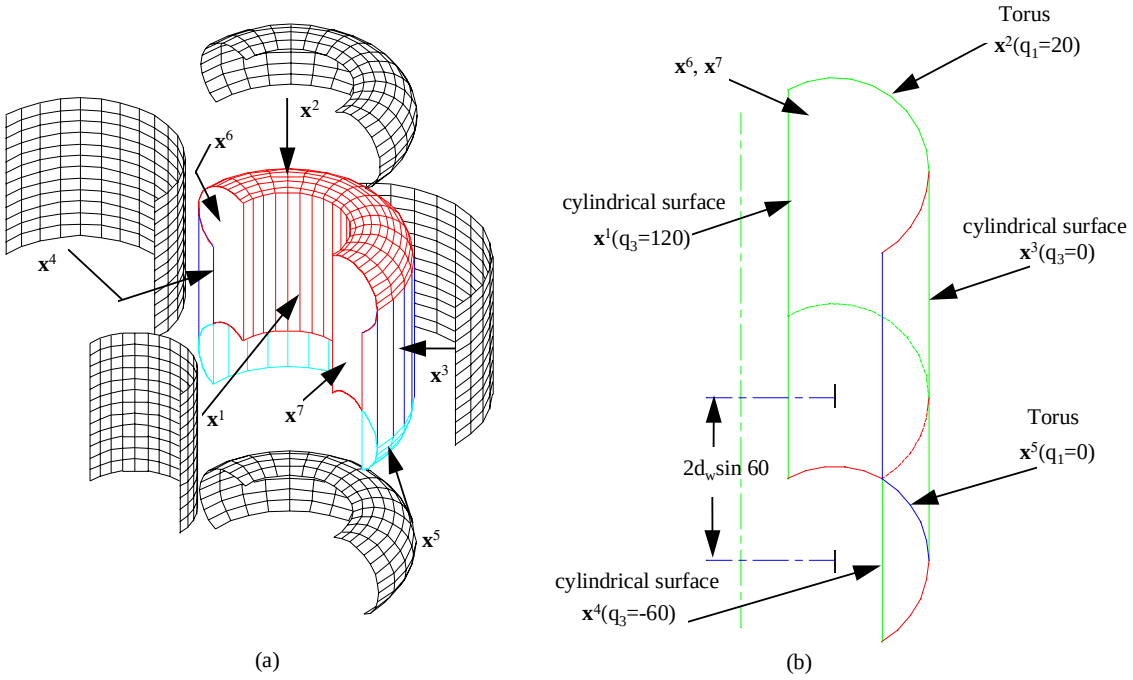

Fig. 6 (a) A section of the wrist-accessible output set
(b) A cross section of the wrist-accessible output set

Note that surfaces $\mathbf{x}^6(q_2 = 0)$ and $\mathbf{x}^7(q_2 = 270^o)$ are planar surfaces. To illustrate the intersection of surfaces to determine second-order singularities, consider the intersection between the cylindrical surface $\mathbf{x}^4(q_3 = -60^o)$ and the torus $\mathbf{x}^5(q_1 = 0)$. The intersection curve between the two surfaces can be computed by solving the equation

$$\mathbf{x}^4 - \mathbf{x}^5 = \mathbf{0} \qquad (38)$$

carrying out the algebra,

$$\cos q_3 = 0.5 \qquad (39)$$

In most cases, however, numerical solutions of equation (38) need be carried out. The resulting points are then parametrized and the second-order singularity is computed. For $q_3 = -60^o$, and $q_1 = 0$, the curve $\mathbf{c}^1$ is a circle with coordinates parametrized as

$$\mathbf{c}^1 = \begin{bmatrix} (0.5d_w + a_2)\cos q_2 \\ (0.5d_w + a_2)\sin q_2 \\ 0 \end{bmatrix} \text{where } 0 \le q_2 \le 270^o \qquad (40)$$

Similarly, the second curve $\mathbf{c}^2$ where $q_3 = 60^o$, and $q_1 = 2d_w \sin 60^o$, the curve is a circle parametrized as

$$\mathbf{c}^2 = \begin{bmatrix} (0.5d_w + a_2)\cos q_2 \\ (0.5d_w + a_2)\sin q_2 \\ 2d_w \sin 60^o \end{bmatrix} \text{where } 0 \le q_2 \le 270^o \qquad (41)$$

The first set ($q_3 = -60^o$, and $q_1 = 0$) are singularities similar to those resulting from equation (27). The set ($q_3 = 60^o$, and $q_1 = 2d_w \sin 60^o$) is a second-order singularity set that has the effect of subdividing the surfaces into subsurfaces Ψ^i. Figure 7 depicts $\mathbf{x}^4$ as having two subsurfaces: Ψ^3 (shown dotted) and Ψ^4 (shown solid). This means that $\mathbf{x}^4$ is segmented to subsurface Ψ^3 on the interval $q_1 \in [2d_w \sin 60 \quad 20]$, and subsurface Ψ^4 on the interval $q_1 \in [0 \quad 2d_w \sin 60]$.

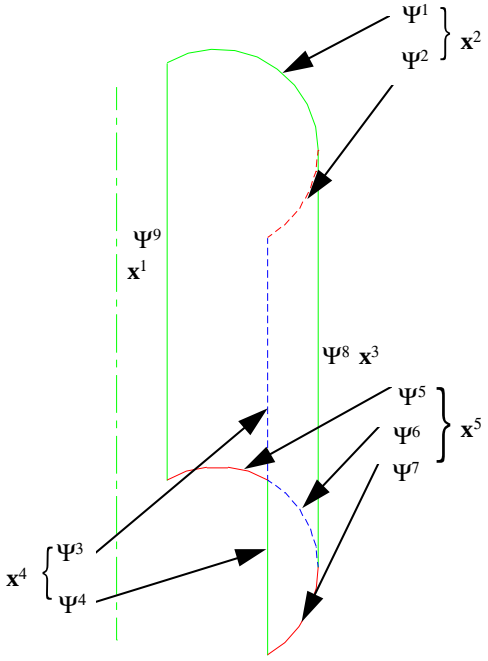

Fig. 7 A cross-section of subsurfaces of the wrist-accessible output set

Similarly, $\mathbf{x}^2$ has two subsurfaces: Ψ^2 on the interval $q_3 \in [-60 \quad 0]$, and Ψ^1 on the interval $q_3 \in [0 \quad 120]$. Surface $\mathbf{x}^5$ has three subsurfaces: Ψ^5 on the interval $q_3 \in [60 \quad 120]$, Ψ^6 on the interval $q_3 \in [0 \quad 60]$, and Ψ^7 on the interval $q_3 \in [-60 \quad 0]$, while the remainder of the surfaces are not subdivided (e.g., $\Psi^8 = \mathbf{x}^3$, $\Psi^9 = \mathbf{x}^1$). Using this method of intersecting surfaces to find second-order singularities, the seven surfaces are divided into 11 subsurfaces (the cross section is depicted in Fig. 7).

To determine whether each subsurface is a boundary or internal subsurface to the wrist-accessible output set, the perturbation method (equation 20) is performed. For example, consider a point on Ψ^1 in the mid range of its interval such that $q_2^o = \left(q_2^{\max} + q_2^{\min}\right)/2 = (0+270)/2 = 135^o$, $q_3^o = \left(q_3^{\max} + q_3^{\min}\right)/2 = (0+120)/2 = 60^o$, and the third component is the singularity at $q_1^o = 20$. Thus, the point on the subsurface is $\mathbf{q}^o = [20 \quad 135 \quad 60]^T$. To determine the unit normal to Ψ^1, we first compute two independent tangent vectors such that

$$\frac{\partial \Psi^1}{\partial q_2} = \begin{bmatrix} -\sin q_2 (d_w \cos q_3 + a_2) \\ \cos q_2 (d_w \cos q_3 + a_2) \\ 0 \end{bmatrix} \tag{42}$$

and

$$\frac{\partial \Psi^1}{\partial q_1} = \begin{bmatrix} -d_w \sin q_3 \cos q_2 \\ d_w \sin q_3 \sin q_2 \\ d_w \cos q_3 \end{bmatrix} \tag{43}$$

and the normal can be evaluated

$$\mathbf{n} = \begin{bmatrix} \cos q_2 (\cos q_3)^2 d_w^2 + \cos q_2 \cos q_3 d_w a_2 \\ \sin q_2 (\cos q_3)^2 d_w^2 + \sin q_2 \cos q_3 d_w a_2 \\ \sin q_3 \cos q_3 d_w^2 + \sin q_3 d_w a_2 \end{bmatrix} \tag{44}$$

then the unit normal $\hat{\mathbf{n}} = \mathbf{n} / \|\mathbf{n}\|$ can be computed at $\mathbf{q}^o$ (on the surface Ψ^1) $\hat{\mathbf{n}}(\mathbf{q}^o) = \begin{bmatrix} -0.354 & 0.354 & 0.866 \end{bmatrix}^T$. Using equation (20), the subsurface Ψ^1 is an internal surface if and only if both perturbations $(\partial\varepsilon = \pm 0.1)$ of $\mathbf{q}^o$ have solutions of the augmented matrix of equation (20) and equation (21). That is

$$\begin{bmatrix} \cos q_2 (\cos q_3 d_w + a_2) - \Psi_x^1(\mathbf{q}^o) - \partial\varepsilon \hat{n}_x \\ \sin q_2 (\cos q_3 d_w + a_2) - \Psi_y^1(\mathbf{q}^o) - \partial\varepsilon \hat{n}_y \\ \sin q_3 d_w + q_1 - \Psi_z^1(\mathbf{q}^o) - \partial\varepsilon \hat{n}_z \\ q_1 - 10 - 10 \sin \lambda_1 \\ q_2 - \frac{3\pi}{4} - \frac{3\pi}{4} \sin \lambda_2 \\ q_3 - \frac{\pi}{6} - \frac{\pi}{2} \sin \lambda_3 \end{bmatrix} = \mathbf{0} \tag{45}$$

For $\partial\varepsilon = -0.1$, there exists a solution to equation (45) such that $\mathbf{q} = \begin{bmatrix} 19.98 & 135 & 60.06 \end{bmatrix}^T$. While for $\partial\varepsilon = +0.1$ no solution can be found. Thus, Ψ^1 is a boundary surface of the wrist-accessible output set and is shown in Fig. 8a.

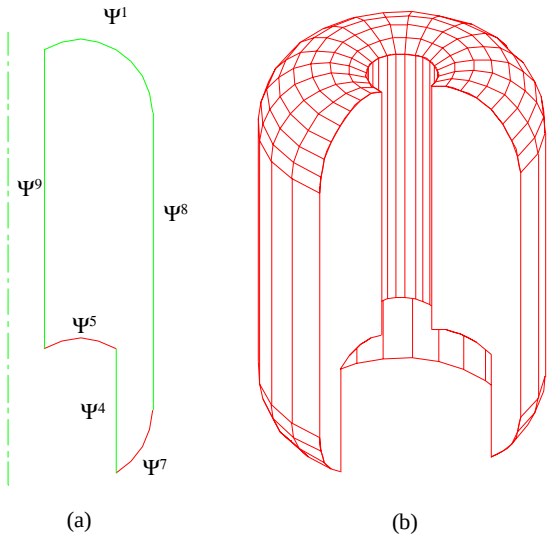

Fig. 8 (a) Boundary subsurfaces of the wrist-accessible output set
(b) The wrist-accessible output set

For subsurface Ψ^2, the point on the mid-range of the inequality constraints is $\mathbf{q}^o = [20 \quad 135 \quad -30]^T$. The normal to this surface at $\mathbf{q}^o$ is $\hat{\mathbf{n}}(\mathbf{q}^o) = [-0.612 \quad 0.612 \quad -0.5]^T$ and, for $(\partial\varepsilon = +0.1)$, there exists a solution to equation (45) such that $\mathbf{q} = [19.98 \quad 135 \quad 60.06]^T$. Thus subsurface Ψ^2 is an internal subsurface. With knowledge of subsurfaces, the boundary of the wrist-accessible output set is determined (depicted in Fig. 8b).

The method described above was used to determine the accessible output set for a number of manipulator configurations. Figures 9a and 9b depict accessible output sets for two combinations of revolute (R) and prismatic (P) joints.

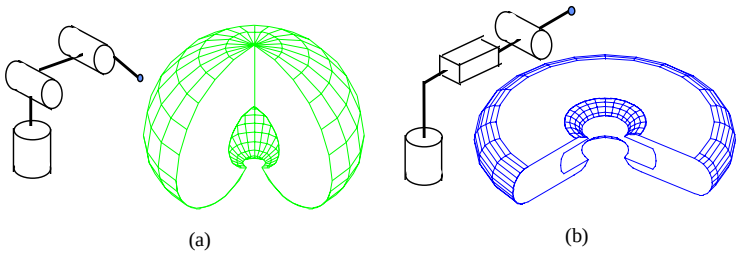

Fig. 9 Wrist-accessible output set (a) RRR, (b) RPR

Finally, the wrist-accessible output set is located with respect to the reference frame at **q** such that the sphere is inside the wrist-accessible output set. This ensures maximum orientability at the operating point **q**. Figure 10 depicts the locality of the manipulator. This step is performed interactively on the computer screen. The location (position vector **v)** and orientation (vectors **n**, **s**, and **a**) are determined. In the case of the manipulator that is analyzed throughout this paper, a suitable orientation of the base of the manipulator is then given by the rotation matrix

$$\mathbf{R} = \begin{bmatrix} \mathbf{n} & \mathbf{s} & \mathbf{a} \end{bmatrix} = \begin{bmatrix} 0 & -1 & 0 \\ 0 & 0 & -1 \\ 1 & 0 & 0 \end{bmatrix} \tag{46}$$

and the position vector $\mathbf{v} = \begin{bmatrix} 0 & 10 & 1.5 \end{bmatrix}^T$.

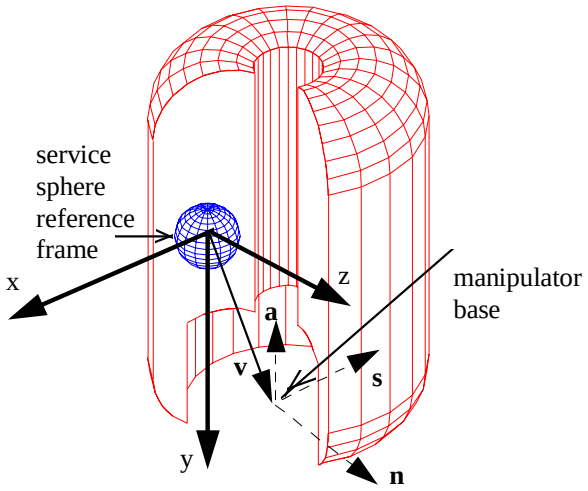

Fig. 10 Determining the locality

The locality chosen by R and v above indicate that the manipulator base should located at a lower horizontal plane than that of the operating point q to obtain maximum orientability as illustrated in Fig. 11a.

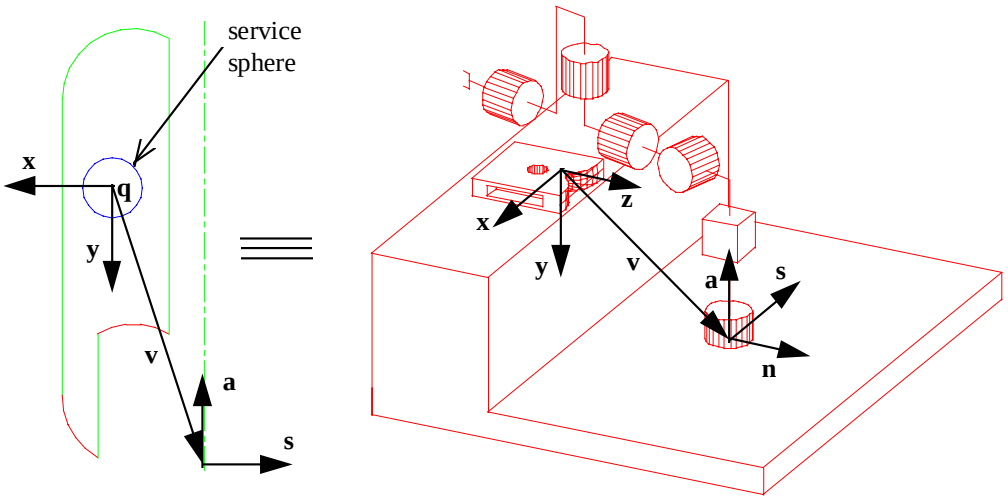

(a)

Fig. 11 (a) Locality of a manipulator determine by the presented method

However, if the manipulator was located on the same horizontal plane as that of the operating point, Fig. 11b illustrates that a significantly less orientability would be obtained.

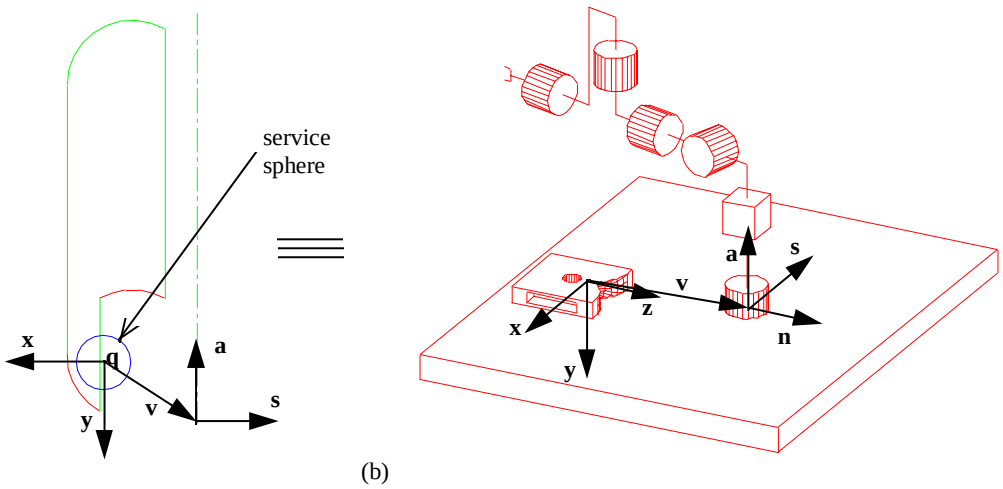

(b)

Fig. 11 (b) Locality of a manipulator at a minimum orientability

4 CONCLUSIONS

The analytical formulation for determining an optimal locality of a manipulator with respect to an operating point, originally contemplated by Abdelmalek **(27),** is shown to be a direct extension of a formulation derived to determine the wrist-accessible output set of a manipulator. Analytical and computational implementation of the formulation presented indicates that it is possible to determine a subspace of the dexterous workspace where the manipulator will have maximum orientability. The formulation presented in this paper is valid for planar as well as spatial manipulators. If the manipulator has more than four DOF, then this formulation requires that the manipulator has a spherical wrist. The method is currently being extended to manipulators including a general form of wrist.

5 ACKNOWLEDGMENTS

The author wishes to extend his thanks to UTI Corporation in Collegeville, PA, for the funding of a larger part of this research and for the use of their equipment and set-up. Many thanks are also due to Professor Burton Paul at the University of Pennsylvania in Philadelphia, PA, for sharing his insights.

6 REFERENCES

1 **Zeghloul, S**., and **Pamanes-Garcia, J.A**. Multi-criteria Optimal Placement of Robots in Constrained Environments. *Robotica*, 1993, **11**:105-110.

2 **Nelson, B., Pederson, K.,** and **Donath, M.** Locating Assembly Tasks in a Manipulator's Workspace. *IEEE Proc. of the Int. Conf. on Robotics and Automation*, 1987, pp. 1367-1372.

3 **Vinagradov, I**., et. al. Details of Kinematics of Manipulators with the Method of Volumes. (in Russian) *Mexanika Mashin*, 1971, No.27-28, pp.5-16.

4 **Roth, B.** Performance Evaluation of Manipulators from a Kinematic Viewpoint. NBS Special Publications No. 459, 1975, pp.39-61.

5 **Kumar, A.,** and **Waldron, K.J**. The Dextrous Workspace. ASME Paper No. 80-DET, 1980.

6 **Tsai, Y.C.,** and **Soni, A.H**. Accessible Region and Synthesis of Robot Arms. *J. of Mech. Design*, 1981, 103:803-811.

7 **Gupta, K.C.,** and **Roth, B.** Design Consideration for Manipulator Workspace. *Journal of Mech. Des. and Transm.*, ASME, 1982, **104**(4):704-712.
8 **Haug, E.J., Adkins, F.A., Qiu, C.C.,** and **Yen, J.** Analysis of Barriers to Control of Manipulators Within Accessible Output Sets. *Proceedings of the 20th Design Automation Conference*, 1994, Minneapolis, MN.
9 **Haug, E.J**., et al. Numerical Algorithms for Mapping Boundaries of Manipulator Workspaces *Proceedings of the 23rd ASME Mechanisms Conference*, 1994, Minneapolis, MN.
10 **Wang, J.Y**., and **Wu, J.K**. Dexterous Workspaces of Manipulators, Part 2: Computational Methods *Mechanics of Structures and Machines*, 1993, 21(4):471-506.
11 **Qiu, C.C., Luh, C.M.,** and **Haug, E.J.** Dexterous Workspaces of Manipulators, Part III: Calculation of Continuation Curves at Bifurcation Points. To appear in *ASME J. of Mechanical Design*, 1995.
12 **Lai, Z.C.** *On the Dexterity of Robotic Manipulators*. Ph.D. Dissertation, University of California, Los Angeles, CA, 1986.
13 **Lai, Z.C**. et. al. The Dexterous Workspace of Simple Manipulators. *IEEE J. Robotics and Automation*, 1988, **4**(1).
14 **Abdelmalek, K**., and **Paul, B**. The Dexterous Solid Angle for Manipulators with a Spherical Wrist. *Proceedings of the 23rd ASME Mechanisms Conference*, Minneapolis, MN, 1994.
15 **Abdelmalek, K**. Dexterity of Manipulator arms at an Operating Point. To appear in *ASME J. of Mech. Design*, 1995.
16 **Yang, D.C.H**., and **Lee, T.W.** On the Workspace of Mechanical Manipulators. *J. of Mechanisms, Transmission and Automation Design*, 1983, 105:62-69.
17 **Gosselin, C,** and **Angeles, J.** Singularity Analysis of Closed Loop Kinematic Chains. *IEEE Trans. on Robotics and Automation*, 1990, **6**(3), pp. 281-290.
18 **Emiris, D.M.,** Workspace Analysis of Realistic Elbow and Dual-Elbow Robot. *Mechanisms and Machine Theory*,1993, **28**(3), pp.375-396.
20 **Agrawal, S.K.** Workspace Boundaries of In-parallel Manipulator Systems. *Int. J. of Robotics and Automation*, 1990, **7**(2): 94-99.
21 **Denavit, J.,** and **Hartenberg, R.S**. A Kinematic Notation for Lower-Pair Mechanisms Based on Matrices. *Journal of Applied Mechanics, ASME,* 1955: 215-221.
22 **McKerrow, P.J**. *Introduction to Robotics*, 1991, Addison Wesley.
23 **Haug, E.J., Wang, J.Y.,** and **Wu, J.K.** Dextrous Workspaces of Manipulators. I. Analytical Criteria. *Mech. Struct. and Mach*. (E.J. Haug, ed.), 1992, **20**(3):321-361.
24 **Qiulin, D.,** and **Davies, B.J.** *Surface Engineering Geometry for Computer-Aided Design and Manufacturing*, 1987, Ellis Horwood Publishers.
25 **Dupont, J.** *Differential Geometry*, 1993, Aarhus Publ., Denmark.
26 **Pieper, D.L.** The Kinematics of Manipulators Under Computer Control. 1968 Stanford Artificial Intelligence Laboratory, Stanford University, AIM 72.
27 **Abdelmalek, K.** *Off-Line Programming Using Commercial CAD Systems, and Design Criteria for Inherently High Accuracy Robots*. Ph.D. Dissertation, University of Pennsylvania, Philadelphia, PA, 1993.

7 LIST OF ILLUSTRATIONS

Fig. 1 (a) Manipulator base at locality 1 and (b) manipulator base at locality 2